

Controlling biomolecular condensates via chemical reactions

Jan Kirschbaum, David Zwicker
Max Planck Institute for Dynamics and Self-Organization
(Dated: March 5, 2021)

Biomolecular condensates are small droplets forming spontaneously in biological cells via phase separation. They play a role in many cellular processes, but it is unclear how cells control them. Cellular regulation often relies on post-translational modifications of proteins. For biomolecular condensates, such chemical modifications could alter the molecular interaction of key condensate components. We here test this idea using a theoretical model based on non-equilibrium thermodynamics. In particular, we describe the chemical reactions using transition-state theory, which accounts for the non-ideality of phase separation. We identify that fast control, like in cell signaling, is only possible when external energy input drives the reaction out of equilibrium. If this reaction differs inside and outside the droplet, it is even possible to control droplet sizes. Such an imbalance in the reaction could be created by enzymes localizing to the droplet. Since this situation is typical inside cells, we speculate that our proposed mechanism is used to stabilize multiple droplets with independently controlled size and count. Our model provides a novel and thermodynamically consistent framework for describing droplets subject to non-equilibrium chemical reactions.

INTRODUCTION

Biomolecular condensates are small droplets that structure the cell interior of eukaryotes [7, 10] and prokaryotes [5, 14, 21]. They form by phase separation and participate in a wide range of cellular functions [2]: Since they are chemically distinct from their surrounding, they can act as reaction centers [35, 42], like the nucleolus inside the nucleus [32]. In particular, locally elevated concentrations can induce polymerization, like in microtubule branching [49] or in centrosomes [59, 64] that additionally control the subcellular organization. Condensates can also store molecules to buffer fluctuations in gene expression [31] or to release them later when the condensate dissolves, like germ granules and the Balbiani body [51]. Condensates also help to detect changes in the environment externally, like receptor clusters [28, 62], and internally, like stress granules [3]. In particular, transcriptional condensates actively regulate gene expression [46]. In all these examples, the cell controls the size, position, or count of the biomolecular condensates [7, 50]. The formation of biomolecular condensates can be described in the framework of liquid-liquid phase separation [27]. This implies that the droplet size is determined by the total amount of droplet material. Moreover, inevitable surface tension driven Ostwald ripening, which is a coarsening process dissolving smaller droplets in favor of larger ones, so that only a single droplet remains in thermodynamic equilibrium. The theory can also be used to predict how the droplet size depends on global parameters, like temperature, pH, and salt concentration [1, 11, 13]. Cells can directly control condensates by changing protein concentrations or molecular interactions [16, 44]. The interactions are mainly dictated by the genetic sequence, which varies on evolutionary time scales. On cellular time scales, post-translational modifications can further adjust the interactions, enabling more dynamic regulation [23, 24]. As an example, phosphorylating the carboxy-terminal domain (CTD) of RNA polymerase II dissolves CTD droplets *in vitro* [8]. More

generally, chemical reactions, like such post-translational modifications, can affect the dynamics of droplets and explain how cells could regulate condensate size, location and count [43, 52].

Theoretical studies of active droplets, which combine phase separation and chemical reactions, suggest that chemical reactions can suppress Ostwald ripening, leading to coexisting droplets of similar size [60, 65] and even droplet division [66]. These studies described chemical reactions using fixed rate laws, which does not include the molecular interactions necessary for phase separation. Instead, a thermodynamically consistent theory is necessary to faithfully describe the interplay of phase separation with reactions. Earlier work in this direction [6, 12, 56] suggests that reactions need to be driven away from equilibrium to be effective.

We here present a minimal model of active droplets, which combines non-equilibrium thermodynamics [15, 30] and transition state theory [22, 41] to describe the chemical reactions. It focuses on chemical potentials as key quantities and describes the non-equilibrium driving explicitly. We identify the conditions under which droplet size control is possible and determine the associated energetic cost. In the following, we build up the complete model by starting from passive liquid-liquid phase separation and we then successively add the reaction, the driving, and enzymatic control.

MODELLING PHASE SEPARATION WITH CHEMICAL TRANSITIONS

We consider an incompressible, liquid mixture of a solvent and a chemical component that can exist in two different forms: a form A , which is soluble in the solvent, and an insoluble form B , which segregates from the solvent. The composition of the system is then given by the volume fractions $\phi_i(\mathbf{x})$ of components $i = A, B$ at each

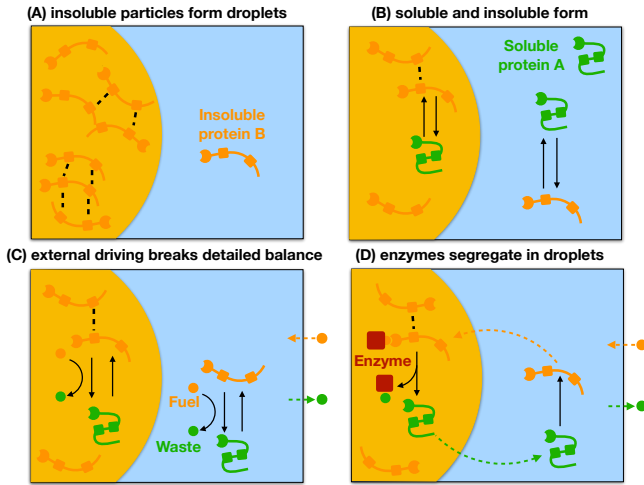


FIG. 1. **Schematic representation of the four discussed models:** (A) B molecules (orange) with weak enthalpic interactions (black dashed lines) form droplets (orange region) that coexist with the dilute phase (blue). (B) A spontaneous chemical transition (black arrow) between the segregating form B and the soluble form A (green) determines the available amount of droplet material B . (C) A second reaction reaction (curved arrow) driven by the conversion of fuel F (orange circle) to waste W (green circle) can lead to a non-equilibrium stationary state when F and W are coupled to particle baths (arrows across box). (D) An enzyme segregating into droplets (red square) controlling the driven reaction causes cyclic diffusive fluxes (dashed arrows) in the system, which can stabilize multiple droplets in the same system.

position \mathbf{x} . They evolve as

$$\partial_t \phi_A = -\nabla \cdot \mathbf{j}_A - s \quad (1a)$$

$$\partial_t \phi_B = -\nabla \cdot \mathbf{j}_B + s, \quad (1b)$$

where \mathbf{j}_i are diffusive fluxes and s is the reactive flux associated with the chemical transition $A \rightleftharpoons B$. We assume that the chemical component cannot leave the system, which implies the normal fluxes $\mathbf{n} \cdot \mathbf{j}_A$ and $\mathbf{n} \cdot \mathbf{j}_B$ vanish at the boundary with normal vector \mathbf{n} . Consequently, the total amount of the chemical component is conserved.

The diffusive and reactive fluxes, \mathbf{j}_i and s , can be described in the framework of non-equilibrium thermodynamics [15], which ensures that a closed system relaxes to thermodynamic equilibrium and that detailed balance is obeyed. One consequence is that the fluxes \mathbf{j}_i and s are related to the chemical potentials $\mu_i(\mathbf{x})$ of the species $i = A, B$. In particular, the diffusive fluxes can be approximated by $\mathbf{j}_i = -\sum_j \Lambda_{ij} \nabla \mu_j$, where the diffusive mobilities Λ_{ij} form the symmetric, positive semi-definite Onsager matrix [15]. In contrast, such a linear approximation is inadequate for the reactive flux s [15] and we thus discuss a more detailed model below.

The chemical potentials $\mu_i(\mathbf{x})$ describe how the free energy F of the system changes when a particle $i = A, B$ replaces an equal volume of solvent at position \mathbf{x} . They are thus given by $\mu_i = v_i \delta F[\phi_A, \phi_B] / \delta \phi_i$, where we consider constant molecular volumes v_i and we assume

$v_A = v_B$. Since the molecular interactions are typically short-ranged, the free energy of this isothermal system of temperature T can be expressed as

$$F[\phi_A, \phi_B] = \int \left[f(\phi_A, \phi_B) - \sum_{i,j=A,B,C} \frac{\kappa_{ij}}{2} \nabla \phi_i \cdot \nabla \phi_j \right] dV, \quad (2)$$

where the integral is over the entire system of volume V_{sys} . Here, f is the local free energy density, which governs phase separation [56]. Conversely, κ_{ij} penalizes composition gradients, which results in surface tension effects [37]. As a concrete example, we consider the free energy density

$$\frac{f(\phi_A, \phi_B)}{k_B T} = \sum_i \frac{\phi_i}{v_i} \ln(\phi_i) + \sum_i e_i \phi_i + \sum_{i,j} \frac{e_{ij}}{2} \phi_i \phi_j, \quad (3)$$

where k_B is Boltzmann's constant and $i, j \in \{A, B, C\}$ using $\phi_C = 1 - \phi_A - \phi_B$. Here, the first term is the mixing entropy and the remaining terms capture enthalpic contributions [19, 26]. In particular, e_i can be interpreted as internal energies, while $e_{ij} = e_{ji}$ capture interactions. Since A molecules are soluble in the solvent, we for simplicity assume that they interact identically to the solvent ($e_{AA} = e_{AC} = e_{CC}$ and $e_{AB} = e_{BC}$). In the special case of a homogeneous system, the chemical potentials then read

$$\mu_A = k_B T \left(w_A + \ln \phi_A - \frac{v_A}{v_C} \ln \phi_C \right) \quad (4a)$$

$$\mu_B = k_B T \left(w_B + \ln \phi_B - \frac{v_B}{v_C} \ln \phi_C - 2\chi \phi_B \right) \quad (4b)$$

where $2\chi = v_B(2e_{BC} - e_{BB} - e_{CC})$ is the Flory parameter capturing relevant interactions and $w_i = 1 - \frac{v_i}{v_C} + v_i(e_i - e_C + e_{iC} - e_{CC})$ quantifies internal energies for $i = A, B$. In non-homogeneous systems, μ_B would also contain a gradient term $\kappa \nabla^2 \phi_B$, where $\kappa = k_B T l^2 \chi$ and l determines the interface width [37]. (1) together with (4) form a typical model for describing phase separation without chemical reactions. We first shortly discuss this classical case and then proceed to examine how different models for the reaction fluxes s affect the droplet formation.

Amount of segregating material determines droplet size

Without chemical reactions ($s = 0$; see Fig. 1A), droplets can form when the free energy F of the demixed system is lower than that of the homogeneous system. This is the case if χ is large enough (see Fig. 2A) while the internal energies w_i are irrelevant since the total amount of each species is conserved [56]. In equilibrium, the diffusive flux \mathbf{j}_B vanishes and the chemical potential μ_B is homogeneous, while ϕ_B can vary strongly. The respective equilibrium fractions ϕ_B^{in} and ϕ_B^{out} inside and outside

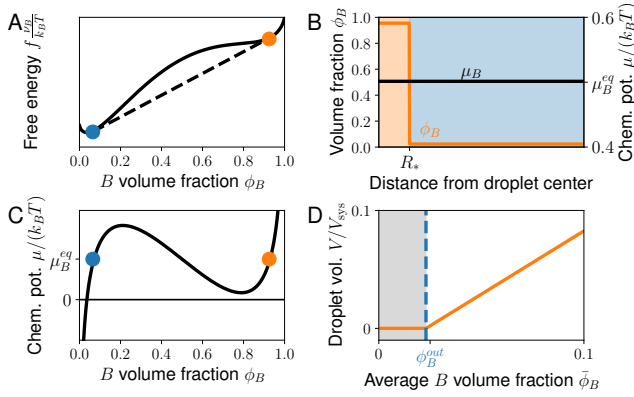


FIG. 2. **The amount of droplet material controls the size of passive droplets.** (A) Free energy density f (Eq.3) as a function of the volume fraction ϕ_B (solid black line). A Maxwell construction (dashed black line) determines the fraction ϕ_B^{in} inside droplets (orange circle) and the fraction ϕ_B^{out} in the solvent (blue circle). (B) Equilibrium volume fraction ϕ_B (left axis) and associated chemical potential μ_B (right axis) as a function of the distance from the droplet center for a single droplet of radius R_* . (C) Chemical potential μ_B as a function of the volume fraction ϕ_B of the droplet material (Eq.4). The chemical potentials are equal at the coexistence point (colored dots). (D) Total volume V of the droplet phase as a function of average fraction $\bar{\phi}_B$ of the droplet material (Eq.5). Droplets do not form for $\bar{\phi}_B < \phi_B^{\text{out}}$ (gray area). Model parameters are $\chi = 3$, $w_B = 0.5$, and $\bar{\phi}_B = 0.026$ (in B).

of the droplet are given by a tangent construction (see Fig. 2A) [37]. They are constant and do not depend on the total composition of the system if the fraction of A is small ($\phi_A \ll 1$). Without reactions, there are only two equilibrium states: Either everything is mixed or a single droplet enriched in B forms. Even if multiple droplets form initially, e.g., due to nucleation, surface tension effects drive coarsening by Ostwald ripening [40] or coalescence, so that all droplets merge into one [56]. The volume V of the droplet follows from material conservation and reads

$$V = \frac{\bar{\phi}_B - \phi_B^{\text{out}}}{\phi_B^{\text{in}} - \phi_B^{\text{out}}} V_{\text{sys}}, \quad (5)$$

where $\bar{\phi}_B = V_{\text{sys}}^{-1} \int \phi_B dV$ is the average fraction of B in the system. Note that the droplet can only exist when $\bar{\phi}_B > \phi_B^{\text{out}}$. All excess material beyond ϕ_B^{out} concentrates in the droplet, so V grows linearly with $\bar{\phi}_B$; see Fig. 2D. A biological cell can thus regulate whether a droplet exists and how large it gets by controlling the total amount of B . Protein amounts can be changed by production and degradation, although this is a costly and slow process. Moreover, V depends on the interaction parameter χ , which is a function of e.g. temperature, pressure, pH, and solvent composition. These parameters are either external to the cell or affect many other processes, so they are not ideal to regulate a specific droplet. Taken together, this analysis shows that additional processes are necessary to control droplets effectively.

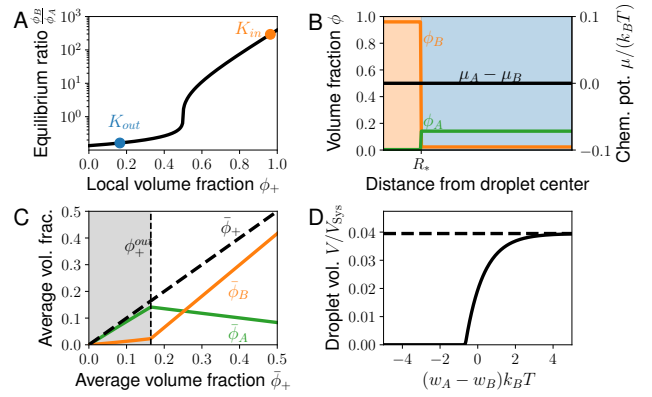


FIG. 3. **Chemical equilibrium sets the amount of droplet material.** (A) The equilibrium ratio of the fractions of soluble and phase separating forms as a function of the total protein fraction $\phi_+ = \phi_A + \phi_B$. (B) Volume fractions ϕ_A and ϕ_B (left axis) and the associated chemical potential difference $\mu_A - \mu_B$ (right axis) as a function of the distance from the center of a droplet of radius R_* . The composition of the droplet (orange shaded area) can differ strongly from the solvent (blue shaded area) even in equilibrium ($\mu_A = \mu_B$). (C) Average volume fractions of A (green line) and B (orange line) as a function of the total average protein volume fraction ϕ_+ in the system. Without droplets (gray area), almost all protein is in the soluble A form, while the opposite is true for large droplets. (D) Total fraction V/V_{sys} occupied by droplets as a function of the difference $w_A - w_B$ between the internal energy of A and B . The dashed line marks the maximal volume, where all proteins are in form B . Model parameters are $\chi = 4$, $w_A - w_B = 2$ (in A, B and C), $\bar{\phi}_+ = 0.2$ (in B) and $\bar{\phi}_+ = 0.06$ (in D)

Chemical reactions control amount of segregating material

A chemical transition that modifies the physical properties of the droplet material can affect droplet formation. Our model captures this when we allow transitions between the soluble form A and the segregating form B of the material. The associated reaction rate s is given by the difference of the rate s^f of the forward reaction $A \rightarrow B$ and the rate s^b of the opposite direction, $s = s^f - s^b$. In the simplest case, the transition $A \rightleftharpoons B$ does not require external energy input (see Fig. 1B), implying the detailed balance condition [56]

$$\frac{s^f}{s^b} = \exp\left(\frac{\mu_A - \mu_B}{k_B T}\right). \quad (6)$$

Chemical equilibrium ($s = 0$) is thus reached when $\mu_A = \mu_B$.

In the simple case of a homogeneous system, the equilibrium state can be characterized by the fractions ϕ_A^{eq} and ϕ_B^{eq} of the two forms. However, since the total fraction $\phi_+ = \phi_A + \phi_B$ of the component is conserved, it is convenient to also discuss the equilibrium constant $K = \phi_B^{\text{eq}}/\phi_A^{\text{eq}}$. Using the chemical equilibrium ($\mu_A = \mu_B$) and Eq. 4, we find $K = \exp(w_A - w_B + 2\chi\phi_B)$, which shows

that K is strongly affected by the difference $w_A - w_B$ of the internal energies of A and B . Note that K is only a constant for an ideal solution ($\chi = 0$). For non-ideal system, K depends on the total fraction ϕ_+ , such that K is larger when there is more material; see Fig. 3A. Taken together, this analysis shows that the chemical equilibrium depends on the environment.

The only inhomogeneous equilibrium state of the system is again a single droplet enriched in B . The analysis of the homogeneous state implies that the ratio $\phi_B^{\text{eq}}/\phi_A^{\text{eq}}$ is larger inside the droplet than outside. This is because the droplet environment favors B over A . Note that A is enriched outside the droplet for the chemical potentials given by Eq. 4 (see Fig. 3B), but more general choices of e_{ij} can enrich A inside the droplet. For our system, ϕ_A is thus dilute in both phases in the common case that the system mostly consists of solvent ($\bar{\phi}_+ \ll 1$), where $\bar{\phi}_+ = V_{\text{sys}}^{-1} \int \phi_+ dV$ denotes the conserved total fraction of A and B . In this case, we can determine the equilibrium fractions of B from the tangent construction given in Fig. 2A since $\phi_A \ll 1$ everywhere. We can then use $K_{\text{in}} = K(\phi_B^{\text{in}})$ and $K_{\text{out}} = K(\phi_B^{\text{out}})$ to determine the total fraction ϕ_+ inside and outside the droplet, $\phi_+^{\text{in}} = (1 + K_{\text{in}}^{-1})\phi_B^{\text{in}}$ and $\phi_+^{\text{out}} = (1 + K_{\text{out}}^{-1})\phi_B^{\text{out}}$. The conservation of $\bar{\phi}_+$ then implies that the droplet volume V is given by

$$V = \frac{\bar{\phi}_+ - \phi_+^{\text{out}}}{\phi_+^{\text{in}} - \phi_+^{\text{out}}} V_{\text{sys}}. \quad (7)$$

Similarly to the case without chemical reactions, a droplet can only form when $\bar{\phi}_+ > \phi_+^{\text{out}}$ and the total amount exceeding the threshold determines the droplet volume. However, the internal energy difference $w_A - w_B$ now also affect the droplet volume; see Fig. 3D. This is mainly because it changes the equilibrium constant K_{out} and thus ϕ_+^{out} . Consequently, external parameters, like temperature, pH, etc., can now affect droplet formation also via the internal energies, thus allowing for a potentially stronger response.

The chemical reactions clearly influence the droplet formation and thus the overall composition in the system. In particular, the relative amounts of A and B strongly depend on whether droplets form or not. Fig. 3C shows that the amount of B in the system increases significantly when the total fraction $\bar{\phi}_+$ exceeds the threshold ϕ_+^{out} so droplets form.

We showed that the chemical transition allows for more detailed control of droplet formation. In particular, the droplet size depends on the total amount of protein, which can again be changed by the slow and costly processes of production and degradation. Additionally, the chemical transition affects droplet size since it determines the ratio of A and B , which is mainly governed by the energy difference $w_A - w_B$. These enthalpic parameters depend on global state variables, like temperature, pH, and salt, as well as on the protein sequence, which can be adjusted only on evolutionary time scales. Consequently, additional processes are necessary to have fast and specific control over droplets.

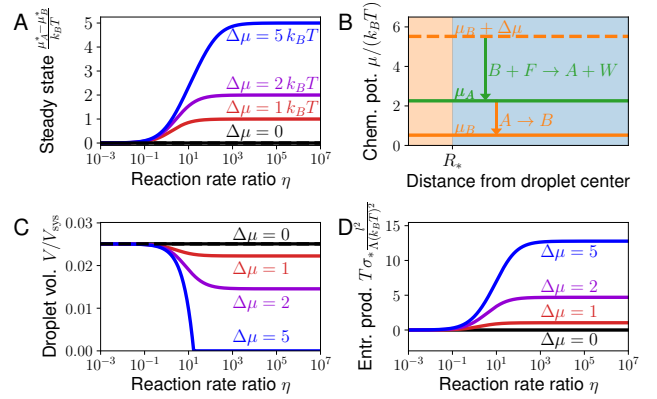


FIG. 4. **A driven transition affects the chemical equilibrium.** (A) Chemical potential difference $\mu_A^* - \mu_B^*$ between A and B as a function of the ratio $\eta = \alpha_1^{-1} \alpha_2 \exp(\mu_F/k_B T)$ of the reaction rate of passive and driven reaction in stationary state for several driving strengths $\Delta\mu$. (B) Chemical potentials of A (green line) and B (solid orange line) as a function of the radial distance from the center of a droplet of radius R_* . The dashed orange line marks the chemical potential difference of the driven reaction, indicating that it spontaneously produces A (green arrow), which is then turned back into B by the passive reaction (orange arrow). Although the system is driven out of equilibrium, the reactions balance locally, so $\nabla\mu_i = 0$. (C) Total fraction V/V_{sys} occupied by droplets as a function of η for different driving strengths $\Delta\mu$. Droplets only vanish completely if the driving is strong enough. (D) Entropy production rate $T\sigma_* = -V_{\text{sys}}s_2\Delta\mu$ in the stationary state as a function of η for different driving strengths $\Delta\mu$. Model parameters are $\chi = 3.5$, $w_A - w_B = 3$, and $\phi_+ = 0.06$

Driven reactions allow enzymatic control of droplets

We next extend our system by allowing the transition $A \rightleftharpoons B$ to also be driven by an external energy input; see Fig. 1C. In particular, we introduce a second reaction, $A + W \rightleftharpoons B + F$, where F and W respectively denote fuel and waste molecules, e.g. ATP and ADP. For simplicity, we consider the case where F and W are dilute and homogeneously distributed, so they do not affect phase separation directly. To keep the system away from equilibrium, we assume that the chemical potential difference $\Delta\mu = \mu_F - \mu_W > 0$ is constant, e.g., because of ATP regeneration. Taken together, $\Delta\mu$ can be interpreted as an ubiquitous external energy source.

The driven reaction obeys the detailed balance condition [56]

$$\frac{s_2^f}{s_2^b} = \exp\left(\frac{\mu_A - \mu_B - \Delta\mu}{k_B T}\right), \quad (8)$$

where s_2^f and s_2^b are the respective forward and backward rates. The net rate $s_2 = s_2^f - s_2^b$ of the driven reaction thus vanishes when $\mu_A - \mu_B = \Delta\mu$. This condition is incompatible with the chemical equilibrium of the passive reaction, $\mu_A = \mu_B$, discussed in the previous section. This implies that the driven system cannot reach thermodynamic equilibrium.

To understand the behavior of the driven system, we first consider stationary states where the total reactive flux, $s = s_1 + s_2$, vanishes. Here, $s_1 = s_1^f - s_1^b$ is the rate associated with the passive reaction, where s_1^f and s_1^b obey the detailed balanced condition given by Eq. 6. Taken together, the condition $s = 0$ requires that the stationary state chemical potentials μ_A^* and μ_B^* obey

$$\mu_A^* - \mu_B^* = \Delta\mu - k_B T \ln \left[\frac{\exp(\Delta\mu/k_B T) + \eta}{1 + \eta} \right], \quad (9)$$

where $\eta = s_2^b/s_1^b$ is the ratio of the backward reaction rates. Note that this condition corresponds to the passive case ($\mu_A^* = \mu_B^*$) for $\eta = 0$, while the driven reaction dominates ($\mu_A^* - \mu_B^* = \Delta\mu$) for $\eta \rightarrow \infty$; see Fig. 4A. In general, we have $0 \leq \mu_A^* - \mu_B^* \leq \Delta\mu$, so that the passive reaction creates the segregating form B while the driven reaction destroys it.

In general, the backward rates s_i^b depend on composition, since they describe the kinetics of the chemical reactions [12]. A simple model for chemical reactions is transition state theory [22, 41], where the forward and backward rates only depend on the chemical potentials of the reactants and products, respectively. Using this theory, we find $s_1^b = \alpha_1 \exp(\mu_B/k_B T)$ and $s_2^b = \alpha_2 \exp[(\mu_B + \mu_F)/k_B T]$, where α_i are constant pre-factors that can be influenced by enzymes; see SI. This implies that $\eta = \alpha_2 \alpha_1^{-1} \exp(\mu_F/k_B T)$, and thus also $\mu_A^* - \mu_B^*$, are constant (see Eq. 9). Taken together with Eq. 1, we thus find that all stationary states with $s = 0$ must have homogeneous chemical potentials; see Fig. 4B.

The driven system can be mapped to the system with passive reactions by altering the internal energies, $w_B \mapsto w_B + (\mu_A^* - \mu_B^*)/k_B T$. Consequently, this system possesses the same stationary states as the passive system, so that at most a single droplet can form and its volume is given by Eq. 7. However, the driven chemical reaction can now be used to control the droplet volume, e.g., by enzymatic activity. For instance, an increased activity of an enzyme that catalyzes the driven reaction corresponds to an increase in α_2 . This results in an increase of η , $\mu_A^* - \mu_B^*$, s , K^{-1} , and ϕ_+^{out} , which leads to a smaller droplet volume V ; see Fig. 4C. Equivalently, raising the external potential $\Delta\mu$ also reduces V . In particular, any change that increases ϕ_+^{out} beyond the average fraction $\bar{\phi}_+$ of available material will dissolve all droplets. Note that this dissolution by enzymatic reactions happens without degrading the material, so droplets could re-form quickly when the original conditions are restored. However, the potential for this quick response comes at the energetic cost, quantified by the entropy production rate (see Fig. 4D), of keeping the droplets dissolved [60].

We showed that at most a single droplet can be stable when the net flux of the chemical reactions vanish everywhere ($s = 0$). To also regulate the droplet count, we thus need inhomogeneous states where $s \neq 0$. However, we show in the SI that there are no stationary states with $s \neq 0$ if η and $\Delta\mu$ are the same everywhere. Consequently, η or $\Delta\mu$ must vary in space to have multiple stable droplets. This could be achieved by imposing spa-

tial heterogeneity, e.g., by producing the fuel or enriching enzymes at particular locations, which would be reflected in the droplet arrangement. Alternatively, the fuel or enzymes can segregate into the droplets spontaneously, which is observed experimentally [8].

Segregated enzymes can control droplet size and count

The main idea to control droplets is to use an enzyme that regulates the chemical transition and segregates into droplets. As an example, we consider an enzyme E that affects the driven reaction; see Fig. 1D. In the simplest case, the rate s_2 of this reaction is proportional to the volume fraction ϕ_E of the enzyme,

$$s_2 = \alpha_2^E \phi_E \left[\exp\left(\frac{\mu_A + \mu_W}{k_B T}\right) - \exp\left(\frac{\mu_B + \mu_F}{k_B T}\right) \right], \quad (10)$$

which follows from Eq. 8 and transition state theory; see SI. Here, α_2^E is a constant pre-factor, so that this case is equivalent to the one discussed in the previous section if ϕ_E is homogeneous.

The distribution of the enzyme will be inhomogeneous if it segregates into droplets. We model this by introducing an additional Flory parameter χ_E , which describes the interaction of the enzyme with the other components; see SI. For simplicity, we consider dilute enzyme concentrations, so it does not affect the phase separation significantly. Consequently, χ_E controls how strongly the enzyme segregates into the droplet [55],

$$\frac{\phi_E^{\text{in}}}{\phi_E^{\text{out}}} \approx e^{\chi_E(\phi_B^{\text{in}} - \phi_B^{\text{out}})}; \quad (11)$$

see SI. In particular, the enzyme is homogeneously distributed for $\chi_E = 0$, corresponding to the case discussed in the previous section.

The enzyme is enriched in the droplet when $\chi_E > 0$. In this case, the driven reaction can stabilize multiple droplets at the same size; see Fig. 5A–B. To understand this behavior, we analyze a single droplet in a large system. Fig. 5D shows that the chemical potentials of A and B are now inhomogeneous even in the stationary state. This implies diffusive fluxes, which are driven by the non-equilibrium chemical reactions: Effectively, inside the droplet, the driven chemical reaction turns the segregating form B into the soluble form A , while form A transitions back to B spontaneously outside. The resulting imbalances between the inside and the outside are compensated by the diffusive fluxes. Consequently, the chemical reactions drive a cycle of diffusive fluxes; see Fig. 1D.

The numerical simulations also show that the stable droplet radius R_* decreases with larger enzyme segregation (larger χ_E); see Fig. 5C. In the stationary state, the diffusive influx J of B toward the droplet is balanced by the reactive flux S of $B \rightarrow A$ inside the droplet ($J = S$). In the simplest case, J is diffusion limited, $J \approx a_1 R$,

while the reaction is homogeneous in the droplet, implying $S \approx a_3 \exp(\chi_E) R_*^3$; see SI. Consequently, the stable radius scales as $R_* \sim \exp(-\frac{1}{2}\chi_E)$. In more realistic cases, the reaction affects the influx J , leading to $J \approx a_2 R_*^2$, which implies $R_* \sim \exp(-\chi_E)$; see Fig. 5E. In both cases, a stable droplet size exists when the fluxes J and S are equal; see Fig. 5E.

The droplet size regulation depends on the non-equilibrium chemical reactions, which maintain a chemical potential difference between the droplet and its surrounding; see Fig. 5D. We observe that the associated entropy production rate σ increases for smaller radii R_* ; see Fig. 5F. This suggests that keeping droplets small consumes more fuel F . In particular, preventing droplet formation ($R_* = 0$) is costly. Conversely, larger droplets require smaller entropy production, although it is still non-zero, similar to the case in the previous section. The fact that droplets reach a stable size implies that multiple droplets can coexist in a larger system. Since all droplets attain the same volume V_* , the number N of droplets is simply $N = V/V_*$, where the total volume V of the droplet phase can be approximated by Eq. 7. In particular, V depends on the total fraction $\bar{\phi}_+$ of A and B , the Flory parameter χ , the internal energies $w_A - w_B$, the driving strength $\Delta\mu$, and the reaction rate ratio η . Conversely, the stable radius V_* is additionally controlled by χ_E , so the droplet count N and the individual volume V_* can be adjusted independently.

DISCUSSION

We introduced a model that explains how chemical reactions can control liquid-like droplets. In particular, we identified three ingredients necessary for effective size control: (i) The chemical modification of the droplet material must convert it to a soluble form, (ii) this modification must involve a driven reaction using a chemical fuel, and (iii) the reaction dynamics must differ inside and outside the droplet, e.g., by localizing enzymes appropriately. The fuel, combined with the imbalance of the reaction, maintains a chemical potential difference between the inside and the outside, which results in sustained diffusive fluxes. This effectively removes droplet material from the droplet, while producing it outside, which explains the stable size of this externally-maintained droplet [56]. In an alternative interpretation, the enzymes enriching in the droplet inhibit further growth, which we already identified as a common motif for size control in biological cells [52].

The stable droplet size R_* predicted by our model is mainly governed by the chemical transition inside the droplet; see SI. In particular, $R_* \sim [3D\Delta c/(k_0 c_E^{\text{in}})]^{1/2}$ where $D \approx 1 \mu\text{m}^2/\text{s}$ is a typical diffusivity [48], while the other parameters can vary widely [38]. Here, Δc quantifies the concentration variation of droplet material B in the dilute phase, k_0 is the catalytic rate constant, and c_E^{in} is the enzyme concentration inside the droplet. For strong reactions ($k_0 \approx 100 \text{s}^{-1}$) and strong

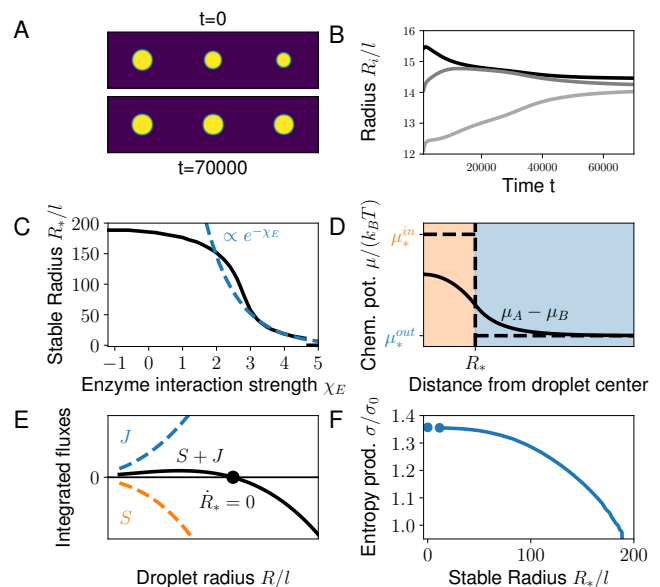


FIG. 5. A segregated enzyme can control and stabilize multiple droplets. (A) Snapshots of a numerical simulation of three droplets in a cylindrical geometry at two time points. Simulation parameters are $\chi = \chi_E = 4$, $w_A - w_B = 2$, $\Delta\mu = 10k_B T$, $\Lambda = 1$, $\alpha_1 = 10^{-3} \Lambda/l^2$, $\eta = 3$, and $\bar{\phi}_+ = 0.25$. (B) Droplet radii R_i of the simulation in (A) as a function of time. (C) Stable droplet radius R_* as a function of the interaction parameter χ_E for the enzyme. (D) The steady state chemical potential difference between A and B as a function of the distance from the droplet center. The chemical potential gradient does not vanish across the interface between droplet (orange) and solvent phase (blue), implying diffusive fluxes. Far away from the droplet, the reactions cancel each other ($s = 0$), while $s < 0$ in the droplet and $s > 0$ in the solvent close to the interface. (E) The reaction flux in the droplet (orange dashed line) and the solvent (blue dashed line) as well as their sum (black dashed line) as a function of the droplet radius. The two fluxes are equal and opposite at the stationary state (black dot). (F) Entropy production rate $T\sigma = -\int s_2 \Delta\mu dV$ associated with (C) as a function of R_* normalized to the entropy production σ_0 for $\chi_E = 0$. Model parameters used in (C-F) are $\chi = 4$, $\bar{\phi}_+ = 0.06$, $\bar{\phi}_E = 0.001$, $\Lambda = 1$, $\alpha_1 = 5 \cdot 10^{-4} \Lambda/l^2$, $\eta = 1/5$, $w_A - w_B = 4$, and $\Delta\mu = 5k_B T$.

enzyme segregation ($\Delta c/c_E^{\text{in}} \approx 0.1$), we find very small droplets ($R_* \approx 0.05 \mu\text{m}$). Conversely, droplets are much larger ($R_* \approx 17.3 \mu\text{m}$) for weaker reactions ($k_0 \approx 0.1 \text{s}^{-1}$) and moderate segregation ($\Delta c/c_E^{\text{in}} = 10$). Consequently, droplets can be stabilized on all length scales relevant to biological cells. In particular, R_* is governed by intrinsic model parameters and is thus independent of system size, similar to other theoretical predictions from combining phase separation with chemical reactions [12, 33, 60, 65]. In all these systems, Ostwald ripening is suppressed and multiple droplets can stably coexist. The droplet count is given by the ratio of the total amount of droplet material and the stable droplet volume.

Whether droplets form and how large they get mainly depends on the available amount of droplet material. Our

model reveals that this key quantity can be regulated on many time scales in biological cells: Adapting the genetic sequence on evolutionary time scales affects the internal energies of the soluble and segregating forms, thus influencing the fraction of droplet material; see Fig. 3D. On the time scale of minutes to hours, protein production and degradation affects the overall composition; see Fig. 2D. Faster time scales are accessible using active processes: By activating and deactivating enzymes, the cell can regulate the reaction rates α_1 and α_2 and thus the balance between the two forms. Note that even small changes in these rates have a huge impact on droplet size when the driving $\Delta\mu$ is sufficiently strong; see Fig. 4C. This active regulation allows cells to quickly adapt their biomolecular condensate in response to internal and external signals [3, 28, 62]. However, this flexibility comes at the cost of continuous turnover of droplet material, reminiscent of enzymatic futile cycles [47]. Moreover, the continuous turnover could prevent the observed aging of biomolecular condensates [4, 29, 34].

Our model unveils the required ingredients for droplet size regulation since it obeys thermodynamic constraints, in contrast to our earlier theory [65]. Similar to electro-

chemical systems [6], the chemical reactions in our system cannot be described by the law of mass action since phase separating solutions are non-ideal. In particular, the associated equilibrium constants differ inside and outside the droplet; see Fig. 3A. To investigate this further, our theory could be extended to client chemical reactions [55], multi-component droplets [44], complex multi-layered droplets [36, 37, 53], and multiple different droplets affecting each other [25], which are all relevant in biological cells. Moreover, it is unclear how active droplets interact with other sub-cellular structures, like the cytoskeleton [58], or generally with the elastic properties of their surrounding [45, 54]. It will be interesting to test our ideas with engineered condensates [9] using fueled chemical reactions [17].

ACKNOWLEDGMENT

We thank Johannes Söding, Estefania Vidal, Christoph A. Weber, and Noah Zietzen for helpful discussions and Lucas Menou for critically reading the manuscript. This work has been supported by the Max Planck Society.

-
- [1] O. Adame-Arana. Liquid Phase Separation Controlled by pH. *biophysical journal*, 119:16, Oct. 2020.
- [2] S. Alberti. The wisdom of crowds: regulating cell function through condensed states of living matter. *Journal of Cell Science*, 130:2789–2796, Sept. 2017.
- [3] S. Alberti and S. Carra. Quality Control of Membraneless Organelles. *Journal of Molecular Biology*, 430(23):4711–4729, Nov. 2018.
- [4] S. Alberti and D. Dormann. Liquid–Liquid Phase Separation in Disease. *Annual Review of Genetics*, 53(1):171–194, Dec. 2019.
- [5] C. A. Azaldegui, A. G. Vecchiarelli, and J. S. Biteen. The Emergence of Phase Separation as an Organizing Principle in Bacteria. *Biophysical Journal*, 119:S0006349520307347, Sept. 2020.
- [6] M. Z. Bazant. Thermodynamic stability of driven open systems and control of phase separation by electroautocatalysis. *Faraday Discussions*, 199:42, 2017.
- [7] J. Berry, C. P. Brangwynne, and M. Haataja. Physical principles of intracellular organization via active and passive phase transitions. *Reports on Progress in Physics*, 81(4):046601, Apr. 2018.
- [8] M. Boehning, C. Dugast-Darzacq, M. Rankovic, A. S. Hansen, T. Yu, H. Marie-Nelly, D. T. McSwiggen, G. Kobic, G. M. Dailey, P. Cramer, X. Darzacq, and M. Zweckstetter. Rna polymerase ii clustering through carboxy-terminal domain phase separation. *Nature Structural & Molecular Biology*, 25(9):833–840, 2018.
- [9] D. Bracha. Probing and engineering liquid-phase organelles. *Nature Biotechnology*, 37:13, 2019.
- [10] C. P. Brangwynne, C. R. Eckmann, D. S. Courson, A. Rybarska, C. Hoegge, J. Gharakhani, F. Jülicher, and A. A. Hyman. Germline p granules are liquid droplets that localize by controlled dissolution/condensation. *Science*, 324(5935):1729–1732, 2009.
- [11] C. P. Brangwynne, P. Tompa, and R. V. Pappu. Polymer physics of intracellular phase transitions. *Nature Physics*, 11(11):899–904, 2015.
- [12] D. Carati and R. Lefever. Chemical freezing of phase separation in immiscible binary mixtures. *Phys. Rev. E*, 56:3127–3136, Sep 1997.
- [13] J.-M. Choi, A. S. Holehouse, and R. V. Pappu. Physical principles underlying the complex biology of intracellular phase transitions. *Annual Review of Biophysics*, 49(1):107–133, 2020. PMID: 32004090.
- [14] M. C. Cohan and R. V. Pappu. Making the Case for Disordered Proteins and Biomolecular Condensates in Bacteria. *Trends in Biochemical Sciences*, 45(8):668–680, Aug. 2020.
- [15] S. De Groot and P. Mazur. *Non-Equilibrium Thermodynamics*. Dover Publications, 1984.
- [16] G. L. Dignon, R. B. Best, and J. Mittal. Biomolecular Phase Separation: From Molecular Driving Forces to Macroscopic Properties. *Annual Review of Physical Chemistry*, 71(1):53–75, Apr. 2020.
- [17] C. Donau, F. Späth, M. Sosson, B. A. K. Kriebisch, F. Schnitter, M. Tena-Solsona, H.-S. Kang, E. Salibi, M. Sattler, H. Mutschler, and J. Boekhoven. Active coacervate droplets as a model for membraneless organelles and protocells. *Nature Communications*, 11(1):5167, Dec. 2020.
- [18] P. J. Flory. Thermodynamics of high polymer solutions. *The Journal of Chemical Physics*, 10(1):51–61, 1942.
- [19] P. J. Flory. Thermodynamics of heterogeneous polymers and their solutions. *The Journal of Chemical Physics*, 12(11):425–438, 1944.
- [20] S. C. Glotzer, E. A. Di Marzio, and M. Muthukumar. Reaction-controlled morphology of phase-separating mixtures. *Phys. Rev. Lett.*, 74:2034–2037, Mar 1995.
- [21] C. Greening and T. Lithgow. Formation and function of bacterial organelles. *Nature Reviews Microbiology*, 18,

- July 2020.
- [22] P. Hänggi, P. Talkner, and M. Borkovec. Reaction-rate theory: fifty years after Kramers. *Reviews of Modern Physics*, 62(2):251–341, Apr. 1990.
- [23] M. Hofweber and D. Dormann. Friend or foe—Post-translational modifications as regulators of phase separation and RNP granule dynamics. *The Journal of Biological Chemistry*, 294(18):7137–7150, May 2019.
- [24] M. Hondele, S. Heinrich, P. De Los Rios, and K. Weis. Membraneless organelles: phasing out of equilibrium. *Emerging Topics in Life Sciences*, 4(3):343–354, Dec. 2020.
- [25] M. Hondele, R. Sachdev, S. Heinrich, J. Wang, P. Vallotton, B. M. A. Fontoura, and K. Weis. DEAD-box ATPases are global regulators of phase-separated organelles. *Nature*, 573(7772):144–148, Sept. 2019.
- [26] M. L. Huggins. Solutions of long chain compounds. *The Journal of Chemical Physics*, 9(5):440–440, 1941.
- [27] A. A. Hyman, C. A. Weber, and F. Jülicher. Liquid-Liquid Phase Separation in Biology. *Annual Review of Cell and Developmental Biology*, 30(1):39–58, Oct. 2014.
- [28] K. Jaqaman. Biomolecular condensates in membrane receptor signaling. *Current Opinion in Cell Biology*, 69:7, 2021.
- [29] L. Jawerth, E. Fischer-Friedrich, S. Saha, J. Wang, T. Franzmann, X. Zhang, J. Sachweh, M. Ruer, M. Ijavi, S. Saha, J. Mahamid, A. A. Hyman, and F. Jülicher. Protein condensates as aging Maxwell fluids. *Science*, 370(6522):1317–1323, Dec. 2020.
- [30] F. Jülicher, S. W. Grill, and G. Salbreux. Hydrodynamic theory of active matter. *Reports on Progress in Physics*, 81(7):076601, July 2018.
- [31] A. Klosin, F. Oltsch, T. Harmon, A. Honigmann, F. Jülicher, A. A. Hyman, and C. Zechner. Phase separation provides a mechanism to reduce noise in cells. *science*, 367:6, Jan. 2020.
- [32] D. L. J. Lafontaine, J. A. Riback, R. Bascetin, and C. P. Brangwynne. The nucleolus as a multiphase liquid condensate. *Nature Reviews Molecular Cell Biology*, 21, Sept. 2020.
- [33] Y. I. Li and M. E. Cates. Non-equilibrium phase separation with reactions: a canonical model and its behaviour. *Journal of Statistical Mechanics: Theory and Experiment*, 2020(5):053206, May 2020.
- [34] M. Linsenmeier, M. Hondele, F. Grigolato, E. Secchi, K. Weis, and P. Arosio. Dynamic arrest and aging of biomolecular condensates are regulated by low-complexity domains, rna and biochemical activity. *bioRxiv*, 2021.
- [35] A. S. Lyon, W. B. Peeples, and M. K. Rosen. A framework for understanding the functions of biomolecular condensates across scales. *Nature Reviews Molecular Cell Biology*, 21, nov 2020.
- [36] S. Mao, M. S. Chakraverti-Wuerthwein, H. Gaudio, and A. Košmrlj. Designing the Morphology of Separated Phases in Multicomponent Liquid Mixtures. *Physical Review Letters*, 125(21):218003, Nov. 2020.
- [37] S. Mao, D. Kuldinow, M. P. Haataja, and A. Kosmrlj. Phase behavior and morphology of multicomponent liquid mixtures. *Soft Matter*, 15:1297–1311, 2019.
- [38] R. Milo and R. Phillips. *Cell Biology by the Numbers*. Garland Science, 2015.
- [39] J. V. Nauman, P. G. Campbell, F. Lanni, and J. L. Anderson. Diffusion of insulin-like growth factor-i and ribonuclease through fibrin gels. *Biophysical Journal*, 92(12):4444 – 4450, 2007.
- [40] W. Ostwald. Studien über die bildung und umwandlung fester körper. *Zeitschrift für Physikalische Chemie*, 22U(1):289 – 330, 01 Feb. 1897.
- [41] I. Pagonabarraga, A. Pérez-Madrid, and J. Rubí. Fluctuating hydrodynamics approach to chemical reactions. *Physica A: Statistical Mechanics and its Applications*, 237(1):205 – 219, 1997.
- [42] W. Peeples and M. K. Rosen. Phase separation can increase enzyme activity by concentration and molecular organization. *bioRxiv*, 2020.
- [43] A. K. Rai, J.-X. Chen, M. Selbach, and L. Pelkmans. Kinase-controlled phase transition of membraneless organelles in mitosis. *Nature*, 559(7713):211–216, July 2018.
- [44] J. A. Riback, L. Zhu, M. C. Ferrolino, M. Tolbert, D. M. Mitrea, D. W. Sanders, M.-T. Wei, R. W. Kriwacki, and C. P. Brangwynne. Composition-dependent thermodynamics of intracellular phase separation. *Nature*, 581(7807):209–214, May 2020.
- [45] K. A. Rosowski, T. Sai, E. Vidal-Henriquez, D. Zwicker, R. W. Style, and E. R. Dufresne. Elastic ripening and inhibition of liquid–liquid phase separation. *Nature Physics*, 16(4):422–425, Apr. 2020.
- [46] B. R. Sabari. Biomolecular condensates and gene activation in development and disease. *Developmental Cell*, 55(1):84 – 96, 2020.
- [47] M. Samoilov, S. Plyasunov, and A. P. Arkin. Stochastic amplification and signaling in enzymatic futile cycles through noise-induced bistability with oscillations. *Proc. Natl. Acad. Sci. USA*, 102(7):2310–2315, 02 2005.
- [48] P. E. Schavemaker, A. J. Boersma, and B. Poolman. How important is protein diffusion in prokaryotes? *Frontiers in Molecular Biosciences*, 5:93, 2018.
- [49] S. U. Setru, B. Gouveia, R. Alfaro-Aco, J. W. Shaevitz, H. A. Stone, and S. Petry. A hydrodynamic instability drives protein droplet formation on microtubules to nucleate branches. *Nature Physics*, 2021.
- [50] W. T. Snead and A. S. Gladfelter. The Control Centers of Biomolecular Phase Separation: How Membrane Surfaces, PTMs, and Active Processes Regulate Condensation. *Molecular Cell*, 76(2):295–305, Oct. 2019.
- [51] C. So, S. Cheng, and M. Schuh. Phase separation during germline development. *Trends in Cell Biology*, 1664, 2021.
- [52] J. Söding, D. Zwicker, S. Sohrabi-Jahromi, M. Boehning, and J. Kirschbaum. Mechanisms for active regulation of biomolecular condensates. *Trends in Cell Biology*, 30:4–14, january 2020.
- [53] P. Swain and S. C. Weber. Dissecting the complexity of biomolecular condensates. *Biochemical Society Transactions*, 48(6):2591–2602, Dec. 2020.
- [54] E. Vidal-Henriquez and D. Zwicker. Theory of droplet ripening in stiffness gradients. *Soft Matter*, 16(25):5898–5905, 2020.
- [55] C. Weber, T. Michaels, and L. Mahadevan. Spatial control of irreversible protein aggregation. *eLife*, 8:e42315, may 2019.
- [56] C. A. Weber, D. Zwicker, F. Jülicher, and C. F. Lee. Physics of active emulsions. *Reports on Progress in Physics*, 82(6):064601, apr 2019.
- [57] R. J. Wheeler and A. A. Hyman. Controlling compartmentalization by non-membrane-bound organelles. *Philosophical Transactions of the Royal Society B: Biological Sciences*, 373(1747):20170193, May 2018.

- [58] T. Wiegand and A. A. Hyman. Drops and fibers — how biomolecular condensates and cytoskeletal filaments influence each other. *Emerging Topics in Life Sciences*, 4:15, 2020.
- [59] J. B. Woodruff. The Centrosome Is a Selective Condensate that Nucleates Microtubules by Concentrating Tubulin. *Cell*, 169:23, 2017.
- [60] J. D. Wurtz and C. F. Lee. Chemical-reaction-controlled phase separated drops: Formation, size selection, and coarsening. *Phys. Rev. Lett.*, 120:078102, Feb 2018.
- [61] J. D. Wurtz and C. F. Lee. Stress granule formation via ATP depletion-triggered phase separation. *New Journal of Physics*, 20(4):045008, apr 2018.
- [62] Y. G. Zhao and H. Zhang. Phase Separation in Membrane Biology: The Interplay between Membrane-Bound Organelles and Membraneless Condensates. *Developmental Cell*, 55(1):30–44, Oct. 2020.
- [63] D. Zwicker. py-pde: A Python package for solving partial differential equations. *Journal of Open Source Software*, 5(48):2158, Apr. 2020.
- [64] D. Zwicker, M. Decker, S. Jaensch, A. A. Hyman, and F. Jülicher. Centrosomes are autocatalytic droplets of pericentriolar material organized by centrioles. *Proceedings of the National Academy of Sciences*, 111(26):E2636–E2645, 2014.
- [65] D. Zwicker, A. A. Hyman, and F. Jülicher. Suppression of ostwald ripening in active emulsions. *Phys. Rev. E*, 92:012317, Jul 2015.
- [66] D. Zwicker, R. Seyboldt, C. A. Weber, A. A. Hyman, and F. Jülicher. Growth and division of active droplets provides a model for protocells. *Nature Physics*, 13:408 EP –, 12 2016.

SUPPLEMENTARY INFORMATION

I. MULTICOMPONENT FREE ENERGY

As a basis for our discussion we use a multicomponent free energy F , which depends on the volume fractions $\Phi = (\phi_1, \dots, \phi_N)$ of all N components according to

$$F[\Phi] = \int \left[f(\Phi) - \sum_{i,j=1}^N \frac{\kappa_{ij}}{2} \nabla \phi_i \cdot \nabla \phi_j \right] dV. \quad (\text{S.1})$$

Here $f(\phi)$ is the free energy density and the $\kappa_{ij} = \kappa_{ji}$ terms includes longer range interaction between species i and j , penalizing concentration gradients[56]. We use a Flory-Huggins like free energy density given by

$$\frac{f(\Phi)}{k_B T} = \sum_i \frac{\phi_i}{v_i} \ln(\phi_i) + \sum_i e_i \phi_i + \sum_{i,j} \frac{e_{ij}}{2} \phi_i \phi_j, \quad (\text{S.2})$$

where the first term is the entropic contribution with constant molecular volume v_i , e_i is the internal energy and $e_{ij} = e_{ji}$ is the enthalpic interaction energy between species i and j .

We discuss incompressible systems only, so $\sum_i \phi_i = 1$ at all times. Using this, we can rewrite the interaction term according to

$$\sum_{i,j} \frac{e_{ij}}{2} \phi_i \phi_j = \sum_i \frac{e_{ii}}{2} \phi_i^2 + \sum_{j \neq i} \frac{e_{ij}}{2} \phi_i \phi_j = \sum_i \frac{e_{ii}}{2} \phi_i + \sum_{j \neq i} \frac{e_{ij} - e_{ii}}{2} \phi_i \phi_j \quad (\text{S.3})$$

and using $2\chi_{ij} = 2e_{ij} - e_{ii} - e_{jj}$, we arrive at

$$\frac{f(\Phi)}{k_B T} = \sum_i \frac{\phi_i}{v_i} \ln(\phi_i) + \sum_i \left(e_i + \frac{e_{ii}}{2} \right) \phi_i + \sum_{i,j} \frac{\chi_{ij}}{2} \phi_i \phi_j. \quad (\text{S.4})$$

Here χ_{ij} shows if species i and j prefer to mix ($\chi_{ij} < 0$) or demix ($\chi_{ij} > 0$) due to enthalpic interactions (where $\chi_{ii} = 0$ by definition). Furthermore, we assume that the gradient term in eq.S.1 is determined by the same interactions as the local free energy, such that $\kappa_{ij} = k_B T l^2 \chi_{ij}$, where l is the characteristic length scale of the interaction[37].

Using Eq.S.1 and S.4, we get the chemical potential according to $\bar{\mu}_i = \frac{\delta F}{\delta N_i}$, which results in

$$\frac{\bar{\mu}_i}{k_B T} = 1 + \ln(\phi_i) + v_i \left(e_i + \frac{e_{ii}}{2} \right) + \sum_{j=1}^N v_i \chi_{ij} \phi_j. \quad (\text{S.5})$$

The incompressibility condition $1 = \sum_i \phi_i$ implies that the diffusion of particles is connected, which we use to replace the N -th species by $\phi_N = 1 - \sum_{i \neq N} \phi_i$. Therefore diffusive fluxes are not driven by the chemical potentials given in Eq.S.5 but by exchange chemical potentials

$$\mu_i = \bar{\mu}_i - \frac{v_i}{v_N} \bar{\mu}_N, \quad (\text{S.6})$$

which describe the energy change when i particles are replaced by the same volume of N particles. For a ternary fluid with $i = A, B, C$ and $N = C$, this results in

$$\frac{\mu_A}{k_B T} = 1 - \frac{v_A}{v_C} + v_A(e_A - e_C + e_{AC} - e_{CC}) + \ln(\phi_A) - \frac{v_A}{v_C} \ln(\phi_C) + \sum_{j \neq C} v_A(\chi_{Aj} - \chi_{AC} - \chi_{Cj})\phi_j, \quad (\text{S.7a})$$

$$\frac{\mu_B}{k_B T} = 1 - \frac{v_B}{v_C} + v_B(e_B - e_C + e_{BC} - e_{CC}) + \ln(\phi_B) - \frac{v_B}{v_C} \ln(\phi_C) + \sum_{j \neq C} v_B(\chi_{Bj} - \chi_{BC} - \chi_{Cj})\phi_j. \quad (\text{S.7b})$$

Now for the special case where B phase separates from A and C and A interacts similar to C , such that $\chi_{AC} = 0$ and $\chi_{AB} = \chi_{BC} = \chi/v_B$, we end up with

$$\frac{\mu_A}{k_B T} = w_A + \ln(\phi_A) - \frac{v_A}{v_C} \ln(\phi_C), \quad (\text{S.8a})$$

$$\frac{\mu_B}{k_B T} = w_B + \ln(\phi_B) - \frac{v_B}{v_C} \ln(\phi_C) - 2\chi\phi_B, \quad (\text{S.8b})$$

with $w_A = 1 - v_A/v_C + v_A(e_A - e_C)$ and $w_B = 1 - v_B/v_C + v_B(e_B - e_C + e_{BC} - e_{CC})$, which is the form we use in the main text.

II. ENZYME SEGREGATION

Here we discuss how a dilute enzyme E distributes in the two phases discussed in the main text. The discussion is similar to the derivation of the segregation coefficient in [55]. Therefore we extend the free energy introduced above by a fourth component $\phi_E \ll 1$.

Assuming $\phi_B \gg \phi_E$ the enzymes exchange chemical potential takes the form

$$\frac{\mu_E}{k_B T} \approx w_E + \ln(\phi_E) - \frac{v_E}{v_C} \ln(\phi_C) - (\chi_E + (v_E/v_B)\chi)\phi_B, \quad (\text{S.9})$$

where $\chi_E = v_E(\chi_{EC} - \chi_{EB})$ determines whether it is energetically favorable for the enzyme to be in the B rich droplet phase ($\chi_E > 0$) or the dilute phase ($\chi_E < 0$).

The maxwell construction discussed in Fig.2 of the main text results in $\phi_B = \phi_B^{\text{in}}/\phi_B^{\text{out}}$ for droplet and solvent phase respectively, with chemical potentials $\mu_B(\phi_B^{\text{in}}) = \mu_B(\phi_B^{\text{out}}) = w_B - \chi$ for $\phi_A \ll 1$ and $v_A = v_B = v_C = v$. Those assumptions allow analytical calculations, but are not necessary and the results apply more generally. With this equal enzyme chemical potential in both phases leads to

$$\ln\left(\frac{\phi_E^{\text{in}}}{\phi_E^{\text{out}}}\right) - \chi_E(\phi_B^{\text{in}} - \phi_B^{\text{out}}) = \frac{v_E}{v} \left(\ln\left(\frac{\phi_C^{\text{in}}}{\phi_C^{\text{out}}}\right) + \chi(\phi_B^{\text{in}} - \phi_B^{\text{out}}) \right). \quad (\text{S.10})$$

For $v_C = v_B$ and $\phi_A \ll 1$, the free energy is symmetric, such that $\phi_B^{\text{in}} + \phi_B^{\text{out}} = 1$ and $\phi_C \approx 1 - \phi_B$. In this case

$$\ln\left(\frac{\phi_C^{\text{in}}}{\phi_C^{\text{out}}}\right) + \chi(\phi_B^{\text{in}} - \phi_B^{\text{out}}) \approx \ln\frac{\phi_B^{\text{out}}}{1 - \phi_B^{\text{out}}} + \chi(1 - 2\phi_B^{\text{out}}) = \mu_B(\phi_B^{\text{out}}) - w_B + \chi = 0, \quad (\text{S.11})$$

such that

$$\frac{\phi_E^{\text{in}}}{\phi_E^{\text{out}}} = \exp(\chi_E(\phi_B^{\text{in}} - \phi_B^{\text{out}})) = \Gamma. \quad (\text{S.12})$$

So the segregation is mostly determined by the strength of phase separation $\phi_B^{\text{in}} - \phi_B^{\text{out}}$ and the different interaction of the enzyme with B and C , χ_E . In the strong phase separation regime, we approximate $\phi_B^{\text{in}} - \phi_B^{\text{out}} \approx 1$ and thus

$$\frac{\phi_E^{\text{in}}}{\phi_E^{\text{out}}} = \exp(\chi_E), \quad (\text{S.13})$$

which is the form we use in the main text for simplicity. So far we have calculated the relative amount of enzyme in droplet and solvent phase. Now we calculate the actual volume fraction in each phase for which we need the average volume fraction, $\bar{\phi}_E$ and the total fraction of droplet phase V/V_{sys} . Because the total amount of enzyme is conserved and the volume fraction in droplet and solvent phase are constant, we get

$$V\phi_E^{\text{in}} + (V_{\text{sys}} - V)\phi_E^{\text{out}} = V_{\text{sys}}\bar{\phi}_E, \quad (\text{S.14})$$

and thus

$$\phi_E^{\text{out}} = \frac{1}{1 - V/V_{\text{sys}}(1 - \Gamma)} \bar{\phi}_E \approx \left(1 + (1 - \Gamma) \frac{V}{V_{\text{sys}}}\right) \bar{\phi}_E, \quad (\text{S.15a})$$

$$\phi_E^{\text{in}} = \frac{\Gamma}{1 - V/V_{\text{sys}}(1 - \Gamma)} \bar{\phi}_E \approx \left(1 + (1 - \Gamma) \frac{V}{V_{\text{sys}}}\right) \Gamma \bar{\phi}_E. \quad (\text{S.15b})$$

For droplet size control we usually assume $\Gamma \gg 1$ and $V/V_{\text{sys}} \ll 1$, which can be used to write $\phi_E^{\text{out}} \approx \bar{\phi}_E$ and $\phi_E^{\text{in}} \approx \Gamma \bar{\phi}_E$ in a first order approximation for the analytical calculations.

III. DETAILED BALANCE OF THE RATES

For a given reaction converting reactants R_i into products P_i , $R_i \rightleftharpoons P_i$, detailed balance relates the forward s^f and backward s^b reaction rate according to

$$\frac{s^f}{s^b} = \exp \left[\frac{\sum_i \mu_{R_i} - \sum_i \mu_{P_i}}{k_B T} \right]. \quad (\text{S.16})$$

Where μ_i is the chemical potential of species i . The total reaction flux $s = s^f - s^b$ then vanishes in equilibrium where $\sum_i \mu_{R_i} = \sum_i \mu_{P_i}$. But detailed balance does not tell us how forward and backward rate look like individually. Here we assume that the forward rate is a function of the forward chemical potential $\mu_F = \sum_i \mu_{R_i}$, $s^f(\mu_F)$, and the backward rate is a function of the backward chemical potential $\mu_B = \sum_i \mu_{P_i}$, $s^b(\mu_B)$. This approximation has the advantage that forward and backward rate have a symmetric form and they depend on the energetics of the species that take part in forward or backward reaction only. In this general form we can rewrite the detailed balance condition according to

$$s^f(\mu_F) \left(-\frac{\mu_F}{k_B T} \right) = s^b(\mu_B) \left(-\frac{\mu_B}{k_B T} \right). \quad (\text{S.17})$$

Assuming that μ_F and μ_B can in general be varied independently, both sides of the equation have to be constant individually and thus

$$s^f(\mu_F) = \alpha \exp \left(\frac{\mu_F}{k_B T} \right), \quad (\text{S.18a})$$

$$s^b(\mu_B) = \alpha \exp \left(\frac{\mu_B}{k_B T} \right). \quad (\text{S.18b})$$

Which is the form we use in the main text.

IV. TRANSITION STATE THEORY

To derive the dynamics in the system we need to calculate the reaction flux for each reaction. But the detailed balance condition used in the main text restricts the ratio of forward s^f and backward s^b only. Here we apply transition state theory (TST) to get an explicit form for s^f and s^b . As an example we consider the reaction $A \rightleftharpoons B$. TST now states that A and B represent local minima in the free energy landscape and the transition from A to be B happens via a saddle point T , which forms an energy barrier between A and B . Assuming that the transition state has a constant energy E^\ddagger , the height of forward and backward barrier are $E^\ddagger - E_A$ and $E^\ddagger - E_B$ respectively. If the molecule is close to thermal equilibrium the transition is thermally activated and the probability to cross the barrier is given by the height of the barrier times the attempt frequency ν given by the vibrational modes of the molecule. In this case the forward and backward rate of a single molecule are given by

$$k^f = \nu_1 \exp \left(-\frac{E^\ddagger - E_A}{k_B T} \right), \quad (\text{S.19a})$$

$$k^b = \nu_1 \exp \left(-\frac{E^\ddagger - E_B}{k_B T} \right). \quad (\text{S.19b})$$

Assuming ν is the same for both states. Note that $E_i = \mu_i - k_B T \ln(\phi_i)$. Each $A(B)$ particle has a probability of $k^f(k^b)$ per unit time to become a $B(A)$ particle. In this case the total forward, s^f , and backward, s^b , rates are given

by the rate per particle, $k^{f/b}$, multiplied by the number of particles, given by the local volume fraction: $s^f = \phi_A k^f$ and $s^b = \phi_B k^b$, which results in

$$s^f = \nu_1 \exp\left(-\frac{E^\dagger - \mu_A}{k_B T}\right), \quad (\text{S.20a})$$

$$s^b = \nu_1 \exp\left(-\frac{E^\dagger - \mu_B}{k_B T}\right), \quad (\text{S.20b})$$

which automatically fulfills the detailed balance condition. Applied to the two reactions discussed in the main text, we end up with

$$s_1 = \nu_1 \exp\left(-\frac{E_1^\dagger}{k_B T}\right) \left(\exp\left(\frac{\mu_A}{k_B T}\right) - \exp\left(\frac{\mu_B}{k_B T}\right)\right) = \alpha_1 \left(\exp\left(\frac{\mu_A}{k_B T}\right) - \exp\left(\frac{\mu_B}{k_B T}\right)\right), \quad (\text{S.21a})$$

$$s_2 = \nu_2 \exp\left(-\frac{E_2^\dagger}{k_B T}\right) \left(\exp\left(\frac{\mu_A + \mu_W}{k_B T}\right) - \exp\left(\frac{\mu_B + \mu_F}{k_B T}\right)\right) = \alpha_2 \exp\left(\frac{\mu_F}{k_B T}\right) \left(\exp\left(\frac{\mu_A - \Delta\mu}{k_B T}\right) - \exp\left(\frac{\mu_B}{k_B T}\right)\right). \quad (\text{S.21b})$$

In this case, the parameter $\eta = \exp(\mu_F/k_B T)\alpha_2/\alpha_1$ becomes a constant as μ_B cancels and we end up as

$$\eta = \frac{\alpha_2 \exp\left(\frac{\mu_F}{k_B T}\right)}{\alpha_1}. \quad (\text{S.22})$$

So η depends on: $\mu_F, \mu_W, E_{1/2}^\dagger$ and $\nu_{1,2}$. So the total reaction flux ends up as

$$\frac{s}{\alpha_1} = \left(\exp\left(\frac{\mu_A}{k_B T}\right) - \exp\left(\frac{\mu_B}{k_B T}\right)\right) + \eta \left(\exp\left(\frac{\mu_A - \Delta\mu}{k_B T}\right) - \exp\left(\frac{\mu_B}{k_B T}\right)\right) \quad (\text{S.23})$$

V. CATALYZED REACTIONS

In a catalyzed reaction the equilibrium is unaffected by the catalyst while the reaction rates are sped up significantly (generally in both directions). Here we use the simple reaction $A + E \rightleftharpoons E_\dagger \rightleftharpoons B + E$, where the catalyst E speeds up the transition between A and B , to describe the transition state theory with catalysts. The total reaction flux is given by $s = s^f - s^b$, where $s^f = \phi_A \phi_E k^f$ and $s^b = \phi_B \phi_E k^b$ and introducing the transition state E_\dagger we get for the individual rates

$$k^f = \alpha \exp\left(-\frac{E_{E_\dagger} - E_A - E_E}{k_B T}\right), \quad (\text{S.24})$$

$$k^b = \alpha \exp\left(-\frac{E_{E_\dagger} - E_B - E_E}{k_B T}\right). \quad (\text{S.25})$$

Here $E_i = w_i + h_i$ contains the internal energy w_i and the enthalpic interactions with the environment h_i of species i . If we assume that the enzyme itself does not change significantly during the reaction, we approximate $h_{E_\dagger} \approx h_E + (h_A + h_B)\delta/2$, where δ describes how much the enthalpy of the protein deviates from the average between state A and B in the transition state. With this approximation we get for the reactive fluxes

$$s = \alpha \phi_E \exp\left(-\frac{w_{E_\dagger} - w_E + (h_A + h_B)\delta/2}{k_B T}\right) \left[\exp\left(\frac{\mu_A}{k_B T}\right) - \exp\left(\frac{\mu_B}{k_B T}\right)\right]. \quad (\text{S.26})$$

Now in general the value of $(h_A + h_B)\delta/2$ can be different inside and outside the droplet, while the enzyme volume fraction is always much larger in the droplet phase compared to the solvent phase $\phi_E^{\text{in}} \gg \phi_E^{\text{out}}$. Oftentimes the role of an enzyme, which catalyzes biochemical reactions, is to bind to the reactant/product molecules and force them into a conformation that is favorable for the reaction (the transition state). In this case the large enzyme 'absorbs' the molecules and the interaction between the molecules and the surrounding becomes negligible. Therefore we neglect the factor $(h_A + h_B)\delta/2$ here and assume the enzymatic reaction rate is constant and limited by the amount of enzyme ϕ_E . If we furthermore assume that the driven reaction is sped up by the enzyme, e.g. in phosphorylation reactions, we end up with

$$s = \alpha_E \phi_E \exp\left(\frac{\mu_F}{k_B T}\right) \left[\exp\left(\frac{\mu_A - \Delta\mu}{k_B T}\right) - \exp\left(\frac{\mu_B}{k_B T}\right)\right], \quad (\text{S.27})$$

which is the form we use in the main text.

VI. STEADY STATES WITH DRIVEN REACTIONS

Here we discuss the steady states for the reaction flux in Eq.S.23 derived in the last section. In this case the total reaction flux $s = s_1 + s_2$ and the fluxes of the individual reactions are

$$s_1 = \alpha_1 \left[\exp\left(\frac{\mu_A}{k_B T}\right) - \exp\left(\frac{\mu_B}{k_B T}\right) \right], \quad (\text{S.28a})$$

$$s_2 = \alpha_2 \exp\left(\frac{\mu_F}{k_B T}\right) \left[\exp\left(\frac{\mu_A - \Delta\mu}{k_B T}\right) - \exp\left(\frac{\mu_B}{k_B T}\right) \right]. \quad (\text{S.28b})$$

Using $\eta = \alpha_2 \alpha_1^{-1} \exp(\mu_F/k_B T)$, $\mu_+ = \mu_A + \mu_B$ and $\mu_- = \mu_A - \mu_B$ we write the total reaction flux as

$$s(\mu_+, \mu_-) = \alpha_1 \exp\left(\frac{\mu_+}{2k_B T}\right) \left[(1 + \eta e^{-\Delta\mu/k_B T}) \exp\left(\frac{\mu_-}{2k_B T}\right) - (1 + \eta) \exp\left(-\frac{\mu_-}{2k_B T}\right) \right]. \quad (\text{S.29})$$

The total flux vanishes if the term in the square brackets vanishes. This is the case if $\mu_- = \mu_-^* = \mu_A^* - \mu_B^* = \Delta\mu - k_B T \ln \left[\frac{\exp(\Delta\mu/k_B T) + \eta}{1 + \eta} \right]$. Note that $\mu_- = 0$ corresponds to the equilibrium of the first reaction and $\mu_- = \Delta\mu$ is the equilibrium chemical potential of the driven reaction. Consequently μ_-^* lies somewhere between 0 and $\Delta\mu$ and is determined by the ratio of the two rates η .

Now we make use of μ_-^* to write the total flux as

$$s(\mu_+, \mu_-) = 2\alpha_1 \left(1 + \eta \exp\left(\frac{-\Delta\mu}{k_B T}\right) \right) \exp\left(\frac{\mu_+ + \mu_-^*}{2k_B T}\right) \sinh\left[\frac{\mu_- - \mu_-^*}{2k_B T}\right], \quad (\text{S.30})$$

which shows that $s = 0$ is equivalent to $\mu_- = \mu_-^*$. Note that the prefactor depends on the value of the sum of chemical potentials $\mu_A + \mu_B$. $\mu_A + \mu_B$ has to be constant in the whole system close to the steady state and depends on the total amount of protein and the value of μ_-^* .

VII. UNIQUENESS OF THE STEADY STATE SOLUTION

First consider the steady state solutions for the sum and difference of the continuity equations for A and B , $\partial_t(\phi_A + \phi_B) = 0$ and $\partial_t(\phi_A - \phi_B) = 0$ (for simplicity $\Lambda_A = \Lambda_B$):

$$\nabla^2(\mu_A + \mu_B) = 0, \quad (\text{S.31})$$

$$\nabla^2(\mu_A - \mu_B) - 2s = 0. \quad (\text{S.32})$$

Where we assume no flux boundary conditions ($\mathbf{n}\nabla\mu_i = \mathbf{0}$ at the boundary). Introducing the notation $\mu_+ = \mu_A + \mu_B$ and $\mu_- = \mu_A - \mu_B$, we see that $\mu_+ = \text{const}$ everywhere. Solving the second equation requires the knowledge of s . In the simplest case we can linearize the total reaction flux derived in the previous section, so $s(\mu_-) \approx \alpha\mu_-$. In this case the equation

$$\nabla^2\mu_- - 2\alpha\mu_- = 0 \quad (\text{S.33})$$

has the trivial solution $\mu_- = 0$. To show that the solution is unique we assume we had two solutions μ_1 and μ_2 . Because the equation is linear, $f = \mu_1 - \mu_2$ is a solution as well. Now we use that

$$\nabla(f\nabla f) = (\nabla f)^2 + f\nabla^2 f = (\nabla f)^2 + 2\alpha f^2. \quad (\text{S.34})$$

Integrating this over the whole volume results in

$$\int_V \nabla(f\nabla f) dV = \int_V (\nabla f)^2 + 2\alpha f^2 dV. \quad (\text{S.35})$$

Applying Gauß integral theorem we arrive at

$$\oint_{\partial V} f\nabla f d\mathbf{S} = \int_V (\nabla f)^2 + 2\alpha f^2 dV. \quad (\text{S.36})$$

Now on the boundary the outward normal of ∇f vanishes and thus the boundary integral over $f\nabla f$ vanishes. But f^2 , 2α and $(\nabla f)^2$ are all non-negative, so that f and ∇f have to vanish everywhere and thus $\mu_1 = \mu_2$.

How about the nonlinear version where s is given by Eq.S.30? First $\mu_+ = \text{const}$ remains necessarily fulfilled, but we need to find the solution for

$$\nabla^2 \bar{\mu}_- - a^2 \sinh[\bar{\mu}_-] = 0, \quad (\text{S.37})$$

with $\bar{\mu}_- = \frac{\mu_- - \mu_-^*}{2k_B T}$ now. We can repeat the same steps as before, but with $\bar{\mu}_-$ instead of f and end up with

$$\oint_{\partial V} \bar{\mu}_- \nabla \bar{\mu}_- d\mathbf{S} = \int_V (\nabla \bar{\mu}_-)^2 + 2\alpha \bar{\mu}_- \sinh[\bar{\mu}_-] dV. \quad (\text{S.38})$$

Now $\sinh(\bar{\mu}_-)$ has the same sign as $\bar{\mu}_-$, so $\sinh(\bar{\mu}_-)\bar{\mu}_- \geq 0$ and thus the only solution is $\bar{\mu}_- = 0$ or $\mu_- = \mu_-^*$.

VIII. REACTION RATE IN DROPLET AND SOLVENT PHASE

In this section we discuss the approximation for the reaction rate s in droplet and solvent phase with enzymes segregating in the droplet phase. The general form for s as a function of μ_+ and μ_- is (Eq.S.30):

$$s(\mu_+, \mu_-) = 2\alpha_1 (1 + e^{-\frac{\Delta\mu}{k_B T} \eta}) e^{\frac{\mu_+ + \mu_-^*}{2k_B T}} \sinh\left[\frac{\mu_- - \mu_-^*}{2k_B T}\right]. \quad (\text{S.39})$$

For the reaction flux outside, we assume that the distance between droplets is large compared to the reaction diffusion length scale. In this case $s^{\text{out}} = 0$ far away from the droplet interface and consequently $\mu_-^{\text{out}} = \mu_-^{*,\text{out}}$. Expanding $\sinh(x) \approx x + \mathcal{O}(x^3)$, we get that

$$s^{\text{out}} \approx \alpha_1 (1 + e^{-\frac{\Delta\mu}{k_B T} \eta}) e^{\frac{\mu_+ + \mu_-^*}{2k_B T}} \left[\frac{\mu_- - \mu_-^*}{k_B T}\right] \quad (\text{S.40})$$

This can be further approximated for strong driving, where $e^{-\frac{\Delta\mu}{k_B T} \eta} \ll 1$ and thus $\mu_-^{*,\text{out}} \approx k_B T \ln(1 + \eta)$:

$$s^{\text{out}} \approx \alpha_1 \sqrt{(1 + \eta) e^{\frac{\mu_+}{k_B T}}} \left[\frac{\mu_-}{k_B T} - \ln(1 + \eta)\right] \quad (\text{S.41})$$

In the droplet phase the driven reaction is sped up by a factor $\Gamma \gg 1$ due to segregation of enzymes. Here we consider the case where $\mu_-^{*,\text{in}} \gg \mu_-(R) > \mu_-^{*,\text{out}}$. In this case we assume that the variation of $\mu_-^{\text{in}}(r)$ is small compared to the difference between $\mu_-^{*,\text{in}} - \mu_-(R)$ (or that the radius R of the droplet is small compared to the reaction diffusion length scale). We then expand s^{in} around $\mu_-(R)$ and get

$$s^{\text{in}} \approx \alpha_1 (1 + e^{-\frac{\Delta\mu}{k_B T} \Gamma \eta}) e^{\frac{\mu_+ + \mu_-^{*,\text{in}}}{2k_B T}} e^{\frac{\mu_-^{*,\text{in}} - \mu_-(R)}{2k_B T}} \left(\frac{\mu_-^{\text{in}} - \mu_-(R)}{2k_B T} - 1\right), \quad (\text{S.42})$$

Which we write as

$$s^{\text{in}} \approx \alpha_1 (1 + \Gamma \eta) e^{\frac{\mu_+ - \mu_-(R)}{2k_B T}} \left(\frac{\mu_-^{\text{in}} - \mu_-(R)}{2k_B T} - 1\right). \quad (\text{S.43})$$

Now we assume strong segregation such that $\Gamma \eta \gg 1$ and we end up with

$$s^{\text{in}} \approx \Gamma \eta \alpha_1 e^{\frac{\mu_+ - \mu_-(R)}{2k_B T}} \left(\frac{\mu_-^{\text{in}} - \mu_-(R)}{2k_B T} - 1\right). \quad (\text{S.44})$$

Note that $\frac{\mu_+ - \mu_-(R)}{2k_B T} = -\frac{\mu_B^{eq}}{k_B T}$ and for the reaction outside

$$s^{\text{out}} \approx \alpha_1 (1 + \eta)^{1/2} e^{\frac{\mu_+}{2k_B T}} \left[\frac{\mu_-}{k_B T} - \ln(1 + \eta)\right]. \quad (\text{S.45})$$

Thereby the reaction flux in both phases takes the form

$$s^{\text{in/out}} = \alpha_{\text{in/out}} (\mu_-^{\text{in/out}} - \mu_{-,0}^{\text{in/out}}), \quad (\text{S.46})$$

where $\alpha_{\text{in/out}}$ is the rate and $\mu_{-,0}^{\text{in/out}}$ is the chemical potential for which $s^{\text{in/out}}$ vanishes. Written out, we get $\alpha_{\text{out}} = \alpha_1 (1 + \eta)^{1/2} e^{\frac{\mu_+}{2k_B T}} / k_B T$ and $\mu_{-,0}^{\text{out}} = k_B T \ln(1 + \eta)$ and $\alpha_{\text{in}} = \Gamma \eta \alpha_1 e^{\frac{\mu_+ - \mu_-(R)}{2k_B T}} / (2k_B T)$ and $\mu_{-,0}^{\text{in}} = \mu_-(R) + 2k_B T$.

IX. CONSTRUCTING A NON-EQUILIBRIUM STEADY STATE SOLUTION

We consider a steady state of a single droplet in a solvent phase. Then the steady state continuity equation for droplet and solvent phase are

$$\Lambda \nabla^2 \mu_+^{\text{in}} = 0 \quad (\text{S.47a})$$

$$\Lambda \nabla^2 \mu_-^{\text{in}} = 2s^{\text{in}} \quad (\text{S.47b})$$

$$\Lambda \nabla^2 \mu_+^{\text{out}} = 0 \quad (\text{S.47c})$$

$$\Lambda \nabla^2 \mu_-^{\text{out}} = 2s^{\text{out}}. \quad (\text{S.47d})$$

We furthermore assume the system to be radially symmetric so that $\mu_{+,-}(r)$ and we have no flux boundary conditions at $r = 0, L$ where L is the radius of the system. Both μ_- and μ_+ have to be continuous across the interface, which together with $\mu_+^{\text{in}} = \text{const}$ and $\mu_+^{\text{out}} = \text{const}$ implies that μ_+ is constant in the whole system. Furthermore we know that at the droplet interface μ_B is fixed by the maxwell construction, thus $\mu_B^{\text{in}}(R) = \mu_B^{\text{out}}(R) = \mu_B^{\text{eq}}$ and thus $\mu_-(R) = \mu_-^R = \mu_+(R) - 2\mu_B^{\text{eq}}$. To get a solution for $\mu_-(r)$, we need the reactive flux s as a function of μ_- . Importantly due to different enzyme content, and thus μ_-^* , in droplet and solvent phase, s^{in} and s^{out} are different. We derived the approximate reaction fluxes inside and outside above, see Eq.S.44 and S.45

$$2s^{\text{out}} \approx 2\alpha_1 \sqrt{(1+\eta)e^{\frac{\mu_+}{k_B T}}} \left[\frac{\mu_- - k_B T \ln(1+\eta)}{k_B T} \right] = \alpha_{\text{out}} (\mu_- - k_B T \ln(1+\eta)). \quad (\text{S.48})$$

Where the rate α_{out} has units per time per $k_B T$. In this case the solution for the chemical potential in the solvent phase is given by

$$\mu_-^{\text{out}}(r) = k_B T \ln(1+\eta) + (\mu_-^R - k_B T \ln(1+\eta)) \frac{R}{r} e^{-(r-R)/\ell_{\text{out}}}, \quad (\text{S.49})$$

where $\ell_{\text{out}}^2 = \Lambda/\alpha_{\text{out}}$ is the (squared) reaction diffusion length scale. We can calculate the total reaction flux outside the droplet S^{out} using Eq.S.48 and the radial profile of μ_-^{out}

$$S^{\text{out}} = 4\pi \int_R^\infty \alpha_{\text{out}}^2 (\mu_-^{\text{out}}(r) - \mu_{-,0}^{\text{out}}) r^2 dr = 4\pi \alpha_{\text{out}}^2 (\mu_-^R - k_B T \ln(1+\eta)) \int_R^\infty r R e^{-(r-R)/\ell_{\text{out}}} dr. \quad (\text{S.50})$$

In the (quasi) steady state[56], the total reaction flux has to be equal to the diffusive flux into/out of the droplet $J = S^{\text{out}}$. And J corresponds to the supply ($J > 0$) or depletion ($J < 0$) of droplet material and thus determines droplet growth.

Plugging in $\mu_-^{\text{out}}(r)$, we get

$$J = 4\pi R \Lambda (\mu_-^R - k_B T \ln(1+\eta)) \left(\frac{R}{\ell_{\text{out}}} + 1 \right). \quad (\text{S.51})$$

So the total diffusive flux into the droplet scales with R for large reaction diffusion length ℓ_{out} and with R^2 for small ℓ_{out} .

Now in the droplet phase, the driven reaction is approximately sped up by a factor of $\Gamma \gg 1$ due to the presence of enzymes. And we derived for the reaction flux in the droplet (see Eq.S.44)

$$2s^{\text{in}} \approx 2\Gamma \eta \alpha_1 e^{\frac{\mu_+ - \mu_-^R}{2k_B T}} \left(\frac{\mu_-^{\text{in}} - \mu_-^R}{2k_B T} - 1 \right) = -\alpha_{\text{in}} \Gamma (2k_B T + \mu_-^R - \mu_-). \quad (\text{S.52})$$

Solving the steady state equation inside the droplet, we get the chemical potential profile inside the droplet which reads

$$\mu_-^{\text{in}}(r) = \mu_-^R + 2k_B T \left(1 - \frac{R}{r} \frac{\sinh(r/\ell_{\text{in}})}{\sinh(R/\ell_{\text{in}})} \right), \quad (\text{S.53})$$

where $\ell_{\text{in}}^2 = \Lambda/(\alpha_{\text{in}} \Gamma)$ is the squared reaction diffusion length scale inside the droplet. For droplets small compared to the reaction diffusion length scale (which is necessary for droplet size control) $R/\ell_{\text{in}} \ll 1$ and $r < R$, we get:

$$\mu_-^{\text{in}} \approx \mu_-^R + \frac{2k_B T}{3\ell_{\text{in}}^2} (R^2 - r^2) = \mu_-^R + \frac{2k_B T \alpha_{\text{in}} \Gamma}{3\Lambda} (R^2 - r^2). \quad (\text{S.54})$$

we can then calculate the total reaction flux in droplet phase, $S^{\text{in}} = 4\pi \int_0^R r^2 s^{\text{in}} dr$:

$$S^{\text{in}} = -4\pi(\alpha_{\text{in}}\Gamma)(2k_{\text{B}}T) \int_0^R r^2 \left(1 - \frac{s_0}{3\Lambda}(R^2 - r^2)\right) dr = -(\alpha_{\text{in}}\Gamma)(2k_{\text{B}}T)V_R \left(1 - \frac{2R^2}{15\ell_{\text{in}}^2}\right). \quad (\text{S.55})$$

For the calculation of the stable droplet radius we assume that $R^2 \ll \ell_{\text{in}}^2$ and call $S^{\text{in}} = S$, such that

$$S \approx -(\alpha_{\text{in}}\Gamma)(2k_{\text{B}}T)V_R. \quad (\text{S.56})$$

The stable droplet radius is then determined by the condition $S + J = 0$, which is given by either

$$-(\alpha_{\text{in}}\Gamma)V_R(2k_{\text{B}}T) + 4\pi R\Lambda(\mu_-^R - k_{\text{B}}T \ln(1 + \eta)) = 0 \quad (\text{S.57})$$

and thus

$$R_*^2 = \frac{3\Lambda}{2\alpha_{\text{in}}\Gamma}(\mu_-^R - k_{\text{B}}T \ln(1 + \eta)) = \frac{3\ell_{\text{in}}^2}{2} \left(\frac{\mu_-^R}{k_{\text{B}}T} - \ln(1 + \eta)\right) \propto \exp(-\chi_E), \quad (\text{S.58})$$

for $\ell_{\text{out}} \gg R$ or for $\ell_{\text{out}} \ll R$

$$-(\alpha_{\text{in}}\Gamma)V_R(2k_{\text{B}}T) + \frac{4\pi\Lambda R^2}{\ell_{\text{out}}}(\mu_-^R - k_{\text{B}}T \ln(1 + \eta)) = 0, \quad (\text{S.59})$$

which corresponds to

$$R_* = \frac{3\ell_{\text{in}}^2}{2\ell_{\text{out}}} \left(\frac{\mu_-^R}{k_{\text{B}}T} - \ln(1 + \eta)\right) \propto \exp(-\chi_E). \quad (\text{S.60})$$

So depending on the reaction diffusion length scale in the dilute phase, the stable droplet radius scales with $R_* \propto \exp(-\chi_E/2)$ ($\ell_{\text{out}} \gg R$) or $R_* \propto \exp(-\chi_E)$ ($\ell_{\text{out}} \ll R$).

X. ENTROPY PRODUCTION RATE

An important quantity to describe non-equilibrium states is the total entropy production rate σ , which vanishes in equilibrium systems, but is always positive in a non-equilibrium state. The entropy production rate measures the local entropy production per unit time. Thereby each thermodynamic process (in our case the two reactions and diffusion) has its own entropy production rate given by the product of the thermodynamic force (here chemical potential differences) and flux (here diffusive flux and reaction rates). For our system the local entropy production rate is given by

$$\sigma = \sum_i -\mathbf{j}_i \cdot \nabla \mu_i + s_1(\mu_A - \mu_B) + s_2(\mu_A - \mu_B - \Delta\mu). \quad (\text{S.61})$$

We are interested in the entropy production rate in the non-equilibrium steady state to quantify the energy cost of the given steady state. In this case all forces and fluxes, and thus the entropy production rate, are time independent. In a first step we discuss the non-equilibrium steady state without segregation of enzymes, where $\mu_-(x, t) = \mu_-^*$, $s_1 = -s_2$ and $\nabla \mu_i = 0$. There the entropy production is just given by [15, 56]

$$\sigma = -s_2(\mu_-^*)\Delta\mu, \quad (\text{S.62})$$

where $s_2(\mu_-^*) < 0$ and $\Delta\mu > 0$ so that $\sigma > 0$ as required. Thereby the steady state flux $s_2(\mu_-^*)$ is given by

$$s_2(\mu_-^*) = -\alpha_2 e^{(\mu_B + \mu_F)/k_{\text{B}}T} \left(\frac{1 - e^{-\Delta\mu/k_{\text{B}}T}}{1 + \eta e^{-\Delta\mu/k_{\text{B}}T}}\right). \quad (\text{S.63})$$

In the case of segregating enzymes, the chemical potential gradients do not vanish anymore and the entropy production is not only determined by the reactions anymore. In the steady state the total entropy production is equal to the external energy input, such that

$$\sigma_* = -\Delta\mu s_2(\mu_-(r), \mu_+), \quad (\text{S.64})$$

but now $\mu_-(r)$ is a more complex function of the radius.

XI. ESTIMATING THE STEADY STATE RADIUS

Here we try to estimate conditions under which droplet size control is possible in cells and the corresponding droplet sizes. We estimate the diffusivity D for proteins in cells to be approximately $0.1 - 10 \mu\text{m}^2/\text{s}$ [48].

Estimating reaction rates and comparing them to our reactions is more difficult, because usually mass action kinetics are used to describe reactions. In addition enzymatic reactions are often described using Michaelis Menten kinetics. Assuming that the substrate (here the droplet material) is abundant, which is the case in the droplet phase, the rate of the enzymatic michaelis menten reaction can be approximated by a single rate $k_{cat} \sim 0.01 - 100 \text{s}^{-1}$ [38]. If the driven reaction dominates in the droplet phase, we can write the total reaction flux as

$$S \approx -k_{cat}\phi_E^{\text{in}}V_R. \quad (\text{S.65})$$

To get the diffusive flux J into the droplet, we make use of the fact that μ_+ is constant to write $\mu_- = \mu_+ - 2\mu_B$ and thus $\mu_-^R - k_B T \ln(1 + \eta) = 2(\mu_{B,*} - \mu_B^R)$. Furthermore we know that ϕ_B is fixed by ϕ_B^{out} at the interface and $\phi_B \approx K/(1 + K)\bar{\phi}_+$ far away from the droplet. The second condition is valid if the reaction flux vanishes far away from the droplet and the total droplet volume is small. If the protein and enzyme are dilute in the solvent phase $\phi_C^{\text{out}} \approx 1$ and the concentration variations are small, we can linearize the chemical potential according to $\mu_B \approx \mu_B(\phi_B^{\text{eq}}) + k_B T \frac{\phi_B - \phi_B^{\text{eq}}}{\phi_B^{\text{eq}}}$.

In total the diffusive flux into the droplet is then given by (see Eq.S.51

$$J \approx 4\pi R \frac{\Lambda k_B T}{\phi_B^{\text{eq}}} \left(\frac{K}{1 + K} \bar{\phi}_+ - \phi_B^{\text{eq}} \right) = 4\pi R D \left(\frac{K}{1 + K} \bar{\phi}_+ - \phi_B^{\text{eq}} \right), \quad (\text{S.66})$$

With $D = \Lambda k_B T / \phi_B^{\text{eq}}$.

In this case the stable radius, determined by $S + J = 0$ is given by

$$-k_{cat}\phi_E^{\text{in}}V_R + 4\pi R D \left(\phi_B^{\text{eq}} - \frac{K}{1 + K} \bar{\phi}_+ \right) = 0 \quad (\text{S.67})$$

with $K \approx (1 + \eta)^{-1} \exp(w_A - w_B)$ and we write $D = \Lambda(\partial_{\phi_B} \mu_B)|_{\phi_B^{\text{eq}}}$.

In this case, the stable droplet radius, for small reaction diffusion length in the dilute phase, is given by

$$R_*^2 = \frac{3D}{k_{cat}} \frac{\Delta\phi_B}{\phi_E^{\text{in}}}, \quad (\text{S.68a})$$

$$R_*^2 = \frac{3D}{k_{cat}} \frac{v_E \Delta c_B}{v_B c_E^{\text{in}}} \quad (\text{S.68b})$$

where the second form, expressed in terms of particle concentration instead of volume fraction, is the one used in the main text. For the rates and diffusivities mentioned above, $k_{cat} \sim 0.01 - 100 \text{s}^{-1}$ and $D \sim 0.1 - 10 \mu\text{m}^2/\text{s}$ and approximating the ration of droplet protein concentration difference to enzyme concentration $\Delta c_B / c_E^{\text{in}} \sim 0.1 - 10$ for $v_E \approx v_B$, we get stable droplet radii on the order of $R_* \sim 10^2 - 10^{-2} \mu\text{m}$.